Aerospace Science and Technology 43 (2015) 71–76

Contents lists available at ScienceDirect

Aerospace Science and Technology

www.elsevier.com/locate/aescte

PID guidance law design using short time stability approach

Mehdi Golestani, Iman Mohammadzaman *,[1]

Department of Electrical Engineering, Malek-Ashtar University of Technology, Tehran, Iran

ARTICLE INFO

Article history:
Received 19 October 2013
Received in revised form 31 January 2015
Accepted 21 February 2015
Available online 2 March 2015

Keywords:
PID guidance law
Control loop dynamics
Short time stability
Circle criterion

ABSTRACT

In this paper, a PID guidance law utilizing short time stability approach is designed considering control loop dynamics. The kinematic model demonstrates a feedback formation so that it can be separated into two parts, a linear time-invariant (LTI) element in forward path, and a time-varying gain in feedback. Thus, the circle criterion can be employed for stability analysis of the guidance loop dynamics and stability conditions give an analytical bound for the flight up time in which stability can be insured. The stability bound of the proposed guidance law is less conservative than proportional navigation (PN) and proportional-derivative navigation (PDN) and proportional-integral navigation (PIN) guidance laws. Also, this approach can be used as a tool to design guidance law parameters. Finally, three-dimensional simulation results demonstrate the effectiveness and robustness of the new guidance law against the maneuvering target.

1. Introduction

Proportional navigation (PN) and its generalizations have been widely utilized in guidance law design due to their simplicity, efficiency and ease of implementation and researchers are trying to improve them [13,20]. Many works have been fulfilled on stability problem using Lyapunov approach [6,17–19]. A new guidance law, utilizing proportional navigation concept and variable structure control, has been proposed in [9]. According to Lyapunov differential inequality; a new guidance law with finite time convergence has been presented in [21]. In all these works; seeker, autopilot, and pursuit dynamics have been assumed as ideal. These methods have shown suitable performances, but in practical applications, the LOS angular rate tends to diverge at the vicinity of the interception if these dynamics are not ideal. Consequently, the pursuit acceleration increases and the guidance loop leads to instability. This divergence may greatly affect the miss distance and it can decrease the guidance loop performance.

In [5,7,12] guidance laws using sliding mode approach have been designed considering control loop dynamics. But in practical application, because of vibration, their uses are limited. Since the guidance law should generate a command which is smooth and without vibration, as in [14,15] guidance algorithms based on second order sliding mode control are designed in order to construct an integrated guidance and control. Since these guidance laws are complicated, their applications are restricted in practical usage. In [2,4], two lead guidance laws have been proposed including pursuit dynamics to achieve zero miss distance, but the noise of guidance loop can dramatically affect these methods and practically, the considered assumptions reduce functionality of these guidance laws. A proportional-integral navigation guidance law has been presented in [8] to neutralize the LOS angular rate containing autopilot and seeker dynamics.

The short time stability means that the system's trajectories remain in a specific region of state space in a determined time interval [10]. Proportional navigation stability and system's trajectories behavior in a determined time interval have been investigated through short time stability approach [11]. The stability of the guidance dynamics has been analyzed by employing the circle criterion and using short time stability method [3].

Since the guidance loop can be modeled as a linear time invariant (LTI) element in forward path and a time-varying gain in feedback, the circle criterion can be a suitable instrument to determine stability region. In this paper, a new PID guidance law is presented using the circle criterion to guarantee stability of guidance loop including the seeker and the autopilot dynamics. The reason of using PID guidance law is to increase the stability region and to compensate the seeker and autopilot lag. The seeker and autopilot dynamics have a significant contribution to guidance loop stability; hence, it is important that stability analysis be fulfilled in spite of these dynamics. Furthermore, the guidance process occurs in a short time, so we employ the short time stability approach. Furthermore, the guidance process is occurred in a short time, so we employ the short time stability approach. Also, the stability

* Corresponding author.
E-mail addresses: mehdi_golestani.11238@yahoo.com (M. Golestani), mohammadzaman@modares.ac.ir (I. Mohammadzaman).
[1] Assistant Professor.

http://dx.doi.org/10.1016/j.ast.2015.02.016
1270-9638/

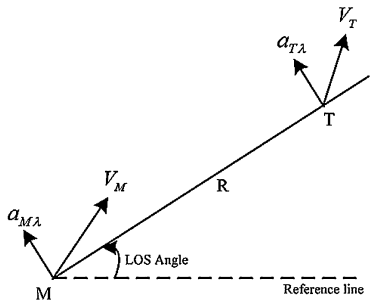

Fig. 1. Planar interceptor–target engagement.

analysis shows that the stability of the proposed guidance law is less conservative than that of the PNG [3], PDNG and PING [8].

Rest of this paper is organized as follows. Section 2 gives the two-dimensional engagement kinematic that is used to analyze PNG systems. The circle criterion and concepts of absolute stability will be presented in Section 3. The stability of proposed guidance law is discussed in Section 4. A three-dimensional design method for guidance law is obtained in Section 5. Some illustrative examples are presented in Section 6, and finally conclusions are given in Section 7.

2. Engagement kinematics

According to the principle of the kinematics, the corresponding equations of motion between the interceptor and target can be described as

$$\ddot{R} = r^2 R + a_{TR} - a_{MR} \tag{1}$$

$$\dot{r} = -\frac{2\dot{R}}{R} r + \frac{a_{T\lambda}}{R} - \frac{a_{M\lambda}}{R} \tag{2}$$

As shown in Fig. 1, R denotes the relative distance between the target and the interceptor; r represents the LOS angular rate; a_{TR} and a_{MR} denote the target and the interceptor acceleration along the LOS, respectively; also $a_{T\lambda}$ and $a_{M\lambda}$ represent the target and the interceptor acceleration normal to the LOS, respectively.

If the interceptor approaches the target with a constant closing velocity of V_C, the range, R, is expressed as

$$R = V_C t_{go} \tag{3}$$

where t_{go} denotes the time to go for the interceptor to hit the target and is defined as below

$$t_{go} = t_f - t \tag{4}$$

$$t_f = R_0 / V_C \tag{5}$$

Using Eq. (3), the nonlinear equation (2) is converted to the following linear equation

$$V_C t_{go} \dot{r} - 2 V_C r = a_{T\lambda} - a_{M\lambda} \tag{6}$$

According to the parallel navigation concept, if LOS direction is kept unchanged with respect to inertial frame and relative range between the interceptor and the target is getting lower ($\dot{R} < 0$), collision will be certain [13]. In other words, the LOS rate must be zero.

In this paper we used a proportional-integral-derivative guidance (PIDG) law as the following equation:

$$a_c = \left(K_1 + \frac{K_2}{s} + K_3 s \right) V_C r_M \tag{7}$$

where K_1, K_2 and K_3 are adjustable constants of guidance law, and r_M represents the LOS angular rate measured by seeker. In a lot of papers, dynamics of the interceptor and the autopilot are considered as ideal, but in practice, neglecting this dynamics in guidance law design causes the guidance loop to lead to instability. Generally the seeker dynamics are modeled by transfer function $G_1(s)$

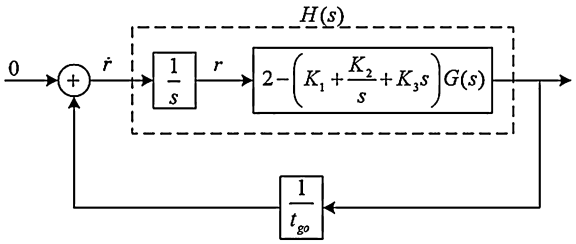

Fig. 2. PID guidance loop.

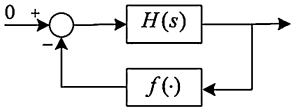

Fig. 3. System under examination.

$$G_1(s) = \frac{r_M(s)}{r(s)} \tag{8}$$

The interceptor's flight control dynamics in closed-loop mode can be described by transfer function $G_2(s)$

$$G_2(s) = \frac{a_{M\lambda}(s)}{a_c(s)} \tag{9}$$

Using Eqs. (7)–(9), the interceptor acceleration is obtained as follows

$$a_{M\lambda}(s) = G_1(s) G_2(s) \left(K_1 + \frac{K_2}{s} + K_3 s \right) V_C r \tag{10}$$

where $G(s) = G_1(s) G_2(s)$ is assumed to be asymptotically stable with $G(0) = 1$.

Now, by substituting Eq. (10) into Eq. (6), the linearized kinematic between the interceptor and the target is obtained by assuming that the target is not maneuvering:

$$t_{go} \dot{r} = \left(2 - \left(K_1 + \frac{K_2}{s} + K_3 s \right) G(s) \right) r \tag{11}$$

In Fig. 2 PID guidance loop consisting of a linear time-invariant (LTI) element $H(s)$ in the forward path and a time-varying gain $1/t_{go}$ in the feedback shown, and it is assumed that $a_{T\lambda} = 0$.

3. Mathematical relations of circle criterion

According to Fig. 3, consider a closed-loop system containing zero input, an LTI transfer function in forward path and a time-varying gain in the feedback. Here we have two assumptions [1]:

A1. In transfer function $H(s) = q(s)/p(s)$, polynomials $p(s)$ and $q(s)$ are coprime, $q(s)$ is monic and system is strictly proper.

A2. The gain $f(\cdot)$ is an operator $f(x,t) : \mathbb{R}^n \times J \to \mathbb{R}_+$, $J \triangleq [t_0, \infty)$ which is a function of the time and maybe state variables, and it is also sufficiently smooth to guarantee the existence and uniqueness of differential equations solution for any initial conditions.

Stability information of closed-loop system after applying circle criterion is obtained and $f(\cdot)$ has the following constraint:

$$0 \le \alpha \le f(x,t) \le \beta < \infty, \quad \forall x \in \mathbb{R}^n, \ \forall t \ge t_0 \tag{12}$$

With these assumptions and applying the circle criterion, the following theorem states sufficient conditions for global absolute stability.

Theorem 1. *The closed-loop system depicted in Fig. 3 with above assumptions is global absolute stable if [1]:*

a) $p(s)+kq(s)$ *has no zeros in the right half-plane* $\mathrm{Re}[s]>0$ *for any* $k\in[\alpha,\beta]$, *and imaginary axis* $\mathrm{Re}[s]=0$ *zeros are simple.*
b) $\mathrm{Re}\{[p(-j\omega)+\alpha q(-j\omega)].[p(j\omega)+\beta q(j\omega)]\}\geq 0, \forall\omega\in\mathbb{R}$.

Using this theorem, sufficient conditions on nonlinear element for closed-loop stability are obtained. Now, suppose that $J_t\triangleq[t_0,t]$. *Consider*

$$f(x,t)=1/(t_f-t),\quad t\in J_{t_f}\triangleq[t_0,t_f] \tag{13}$$

In this case, because of the definition time over a finite interval, we can state the following definition.

Definition 1. System (11) is globally absolutely stable (asymptotically stable) in the interval $J_{t^*}\triangleq[t_0,t^*]\subseteq J_{t_f}$, if there exists $P>0$ such that $\|x\|_P$ is a nonincreasing (decreasing) function of time $\forall x(t_0)$, $\forall t\in J_{t^*}$ [3].

4. Stability of PID guidance

The circle criterion is an instrument of stability analysis, and it can be used to design aims. We can utilize the circle criterion to constrain upper bound and lower bound of the nonlinear element $f(x,t)$.

Based on Fig. 2, we can write

$$H(s)=\frac{q(s)}{p(s)}=\frac{1}{s}\left(2-\left(K_1+\frac{K_2}{s}+K_3 s\right)G(s)\right) \tag{14}$$

Also the nonlinear element $f(x,t)$ is

$$0\leq\alpha=1/t_f\leq 1/t_{go}\leq\beta \tag{15}$$

where $t_{go}=1/\beta$ is the shortest time to go for which the guidance loop of Fig. 2 to be stable. So it is important to calculate β to guarantee guidance loop stability. In order to use Theorem 1, necessary assumptions must be examined. First, we must show that $p(s)$ and $q(s)$ are coprime. This will be done using the following lemma.

Lemma 1. *Consider* $G(s)=n(s)/d(s)$ *with* $n(s)$ *and* $d(s)$ *coprime. Based on Eq. (14) in* $H(s)=q(s)/p(s)$, $p(s)$ *and* $p(s)$ *are coprime if*

$$n(s)|_{s=0}\neq 0 \tag{16}$$

$$d(s)|_{s=\frac{-K_1\pm\sqrt{K_1^2-4K_2K_3}}{2K_3}}\neq 0 \tag{17}$$

$$K_2\neq 0 \tag{18}$$

Proof. See Appendix A. □

We are about to test the results of conditions (a) and (b) of Theorem 1 which declares that frozen time closed-loop system has to be stable for any time in the interval J_{t^*}.

Consider the characteristic equation of the closed-loop system shown in Fig. 3, where the time-varying gain is frozen at a value $k\in[\alpha,\beta]$

$$1+kH(s)=1+\left(\frac{k}{s}\right)\left(2-\left(K_1+\frac{K_2}{s}+K_3 s\right)G(s)\right) \tag{19}$$

Assume that $G(s)=n(s)/d(s)$ is

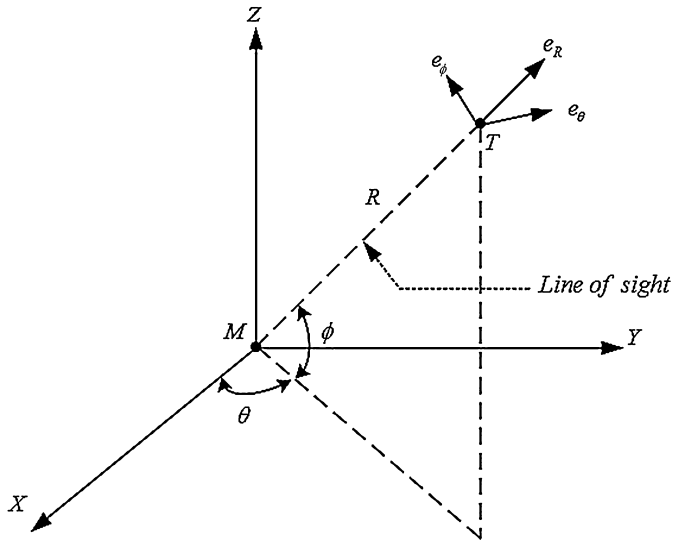

Fig. 4. Three-dimensional interceptor–target geometry.

$$n(s)=a_{n-j}s^{n-j}+a_{n-j-1}s^{n-j-1}+\ldots+a_1 s+a_0 \tag{20}$$

$$d(s)=b_n s^n+b_{n-1}s^{n-1}+\ldots+b_1 s+b_0 \tag{21}$$

where j is the difference between the degree of the numerator and the degree of the denominator. Now, substituting Eqs. (20) and (21) into Eq. (19) yields

$$s^2 d(s)-2ksd(s)+kK_1 sn(s)+kK_2 n(s)+kK_3 s^2 n(s)=0 \tag{22}$$

Assume A_1 is obtained by checking the necessary and sufficient conditions for the frozen system (22) to hold condition (a) in Theorem 1. Obviously, it is necessary that

$$b_{n-i-2}-2kb_{n-i-1}+kK_1 a_{n-j-i-1}+kK_2 a_{n-j-i}+kK_3 a_{n-j-i-2}>0 \tag{23}$$

where $i=0,1,\ldots,n$. So, this condition can constrain k and, therefore, it can constrain t_{go}. Stability condition (23) is obtained due to freezing the nonlinear element.

After examining the Routh–Hurwitz test for the frozen system (22) (i.e., all coefficients are present and positive and the first column of the Routh array has no sign changes), the condition (b) in Theorem 1 should be examined. In [3], it has been proved that the stability condition of system shown in Fig. 3 with linear time invariant element $H(s)$ in forward path and nonlinear element $1/t_{go}$ in feedback has the following relation:

$$t_{go}\geq-\frac{\mathrm{Re}[H(j\omega)]+\alpha|H(j\omega)|^2}{1+\alpha\,\mathrm{Re}[H(j\omega)]},\quad\forall\omega\neq 0 \tag{24}$$

A set of calculations result in

$$t_{go}\geq\max_{\omega}\left\{\frac{-K_1\,\mathrm{Re}[G(j\omega)/j\omega]+(K_2/\omega^2)\,\mathrm{Re}[G(j\omega)]-K_3\,\mathrm{Re}[G(j\omega)]+\alpha|H(j\omega)|^2}{1-\alpha K_1\,\mathrm{Re}[G(j\omega)/j\omega]+(\alpha K_2/\omega^2)\,\mathrm{Re}[G(j\omega)]-\alpha K_3\,\mathrm{Re}[G(j\omega)]}\right\} \tag{25}$$

Assume A_2 is the stability condition of (25). Therefore, the normalized conditions can be stated as $\delta_f=A_1/t_f$ and $\delta=A_2/t_f$, respectively, and they will used in the simulation section.

5. Guidance law design in a three-dimensional model

A three-dimensional interceptor–target engagement is demonstrated in Fig. 4, where the origin is fixed at the interceptor's gravity center. The target and interceptor are modeled as point masses

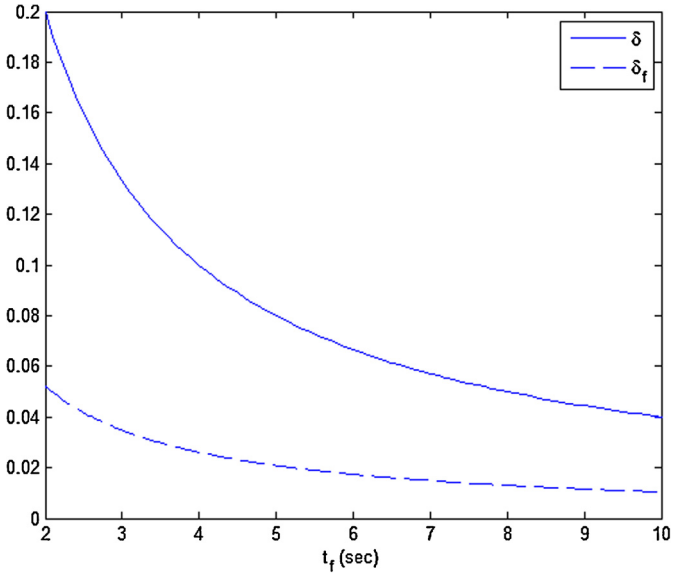

Fig. 5. Plots of the normalized stability condition of frozen system δ and δ_f.

in order to analyze the guidance law. The kinematic equations are presented by [16]

$$\ddot{R} - R\dot{\phi}^2 - R\dot{\theta}^2\cos^2\phi = a_{TR} - a_{MR} \tag{26}$$

$$R\ddot{\theta}\cos\phi + 2\dot{R}\dot{\theta}\cos\phi - 2R\dot{\phi}\dot{\theta}\sin\phi = a_{T\theta} - a_{M\theta} \tag{27}$$

$$R\ddot{\phi} + 2\dot{R}\dot{\phi} + R\dot{\theta}^2\sin\phi\cos\phi = a_{T\phi} - a_{M\phi} \tag{28}$$

where R denotes the relative distance between the target and the interceptor, θ and ϕ represent yaw and pitch LOS angles, respectively. Also, $[a_{Tr}, a_{T\theta}, a_{T\phi}]^T$ and $[a_{Mr}, a_{M\theta}, a_{M\phi}]^T$ denote the acceleration vectors of the target and the interceptor, respectively.

Considering Eqs. (27) and (28) to design a guidance law. It is evident that these equations are coupled. If the Pitch LOS angle is a small variable, it yields $\sin\phi \approx 0$ and $\cos\phi \approx 1$, and then the decoupled three-dimensional kinematic equation will be similar to two-dimensional kinematic equation [21].

According to the results gained in previous section, the two planer guidance laws can be derived as

$$a_{M\theta}(s) = G_1(s)G_2(s)\left(K_1 + \frac{K_2}{s} + K_3 s\right)V_C\dot{\theta} \tag{29}$$

$$a_{M\phi}(s) = G_1(s)G_2(s)\left(K_1 + \frac{K_2}{s} + K_3 s\right)V_C\dot{\phi} \tag{30}$$

6. Illustrative examples

In this section, we consider examples that illustrate the performance of the proposed guidance law and compare it with PNG, PDNG and PDNG. The simulation results are presented in two sections, linear simulation and nonlinear simulation.

6.1. Linear simulation

In linear simulation we plan to analyze the stability regions. Consider an interceptor whose dynamics are modeled by a third-order transfer function

$$G(s) = \frac{1}{(1+\tau_1 s)(1 + 2\zeta s/\omega_n + s^2/\omega_n^2)}$$

If $\zeta = 0.5$, $\tau_1 = 0.3$, $K_3 = 0.6$, $K_2 = 1$, $K_1 = 3$ and $\omega_n = 10$, we can derive the stability conditions. Let A_1 be the stability condition

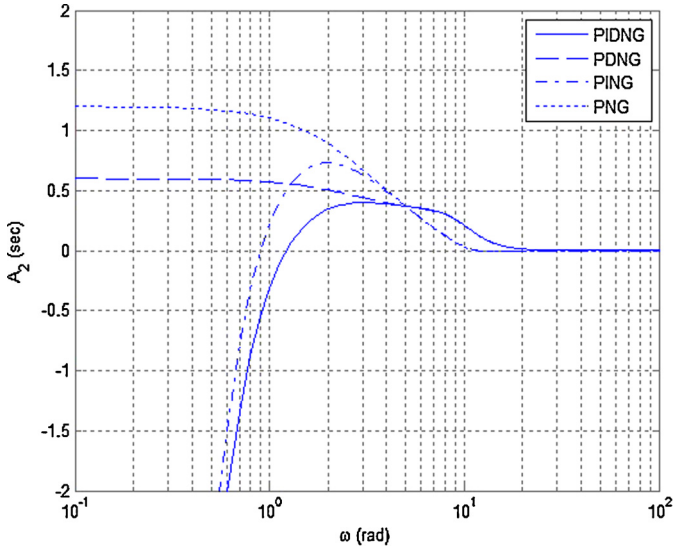

Fig. 6. Plots of condition A_2 for different guidance laws.

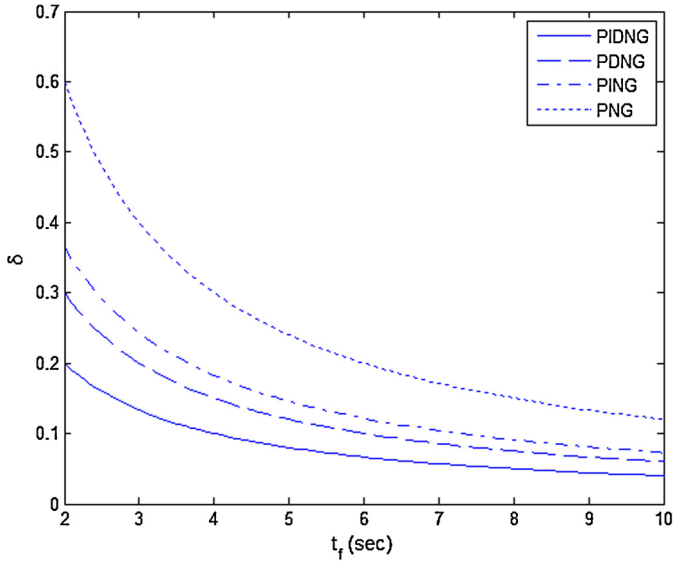

Fig. 7. Plots of the normalized stability condition of frozen system δ with respect to flight time for different guidance laws.

of frozen system (22) and A_2 be the stability condition of (25), therefore, the normalized conditions are stated as $\delta_f = A_1/t_f$ and $\delta = A_2/t_f$, respectively.

In Fig. 5, δ_f and $\delta = A_2/t_f$ are demonstrated with respect to the flight time. By virtue of Fig. 5, it is explicit that the stability condition (24) is more conservative than the requirement of the system closed-loop frozen time stability, and stability examination of frozen system to guarantee the stability of closed-loop system is not sufficient.

In Fig. 6, the stability condition A_2 as a function of the above parameters and $\alpha = 0$ has been shown. Fig. 6 illustrates that the maximum of stability condition in PIDNG is less than PNG, PDNG and PING. So, the stability range in condition A_2 will increase.

In Fig. 7 the normalized stability condition (25) for different guidance laws has been depicted. Fig. 7 also represents that the proposed guidance law has a greater range of stability than PNG, PDNG and PING.

In Fig. 8 the stability condition A_2 as a function of autopilot damping ratio for different guidance laws has been shown. Also Fig. 8 can be used to design autopilot damping ratio. For instance,

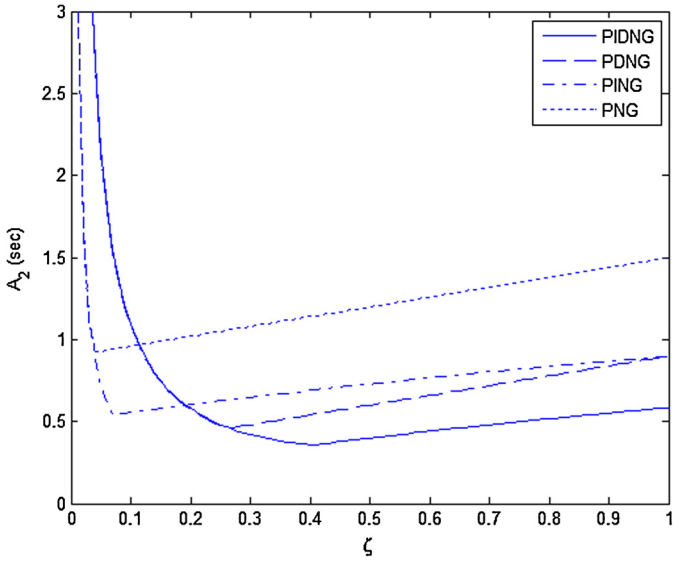

Fig. 8. Plots of condition A_2 with respect to autopilot damping ratio for different guidance laws.

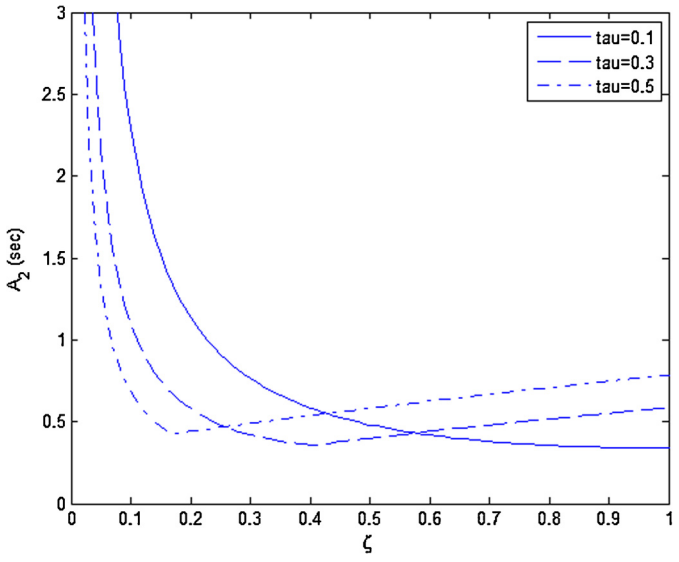

Fig. 9. Plots of condition A_2 as a function of seeker time constant with respect to autopilot damping ratio.

for a system with $K_1 = 3, K_2 = 1, K_3 = 0.6$, if $\zeta = 0.4$, the greatest stability range of the guidance loop will be obtained.

In Fig. 9 the stability condition A_2 as a function of autopilot damping ratio for different values of seeker time constant has been depicted. In Fig. 10 the stability condition A_2 as a function of autopilot damping ratio for different values of autopilot natural frequency has been shown.

6.2. Nonlinear simulation

Since most practical guidance processes are applied in a three-dimensional environment, in this section, the nonlinear equations of three-dimensional relative motion in Eqs. (26)–(28) are considered and the proposed guidance laws in Eqs. (29) and (30) are applied. Furthermore, the results have been compared with PNG, PDNG and PING.

Initial conditions are taken as: $R_0 = 5$ km, $\dot{R}_0 = -500$ m/s, $\theta_0 = 10$ deg, $\dot{\theta}_0 = 0.57$ deg/s, $\phi_0 = 20$ deg, $\dot{\phi}_0 = 1.15$ deg/s. Consider the target flees with constant acceleration components $a_{TR} = 5$ m/s^2,

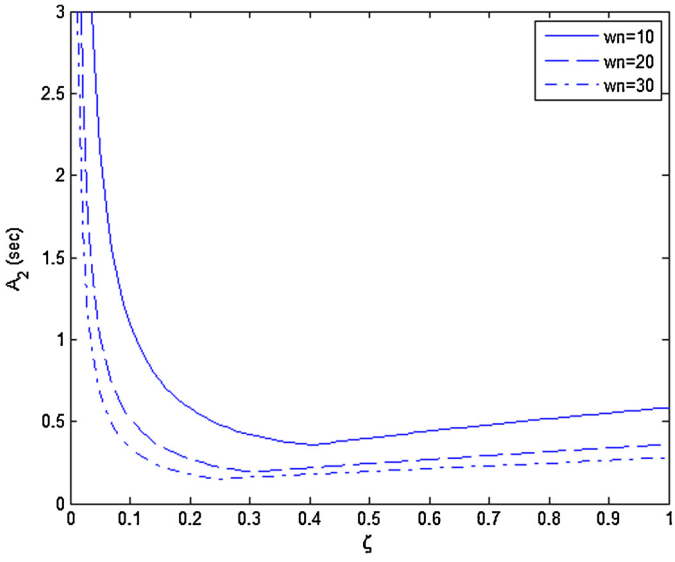

Fig. 10. Plots of condition A_2 as a function of autopilot natural frequency with respect to autopilot damping ratio.

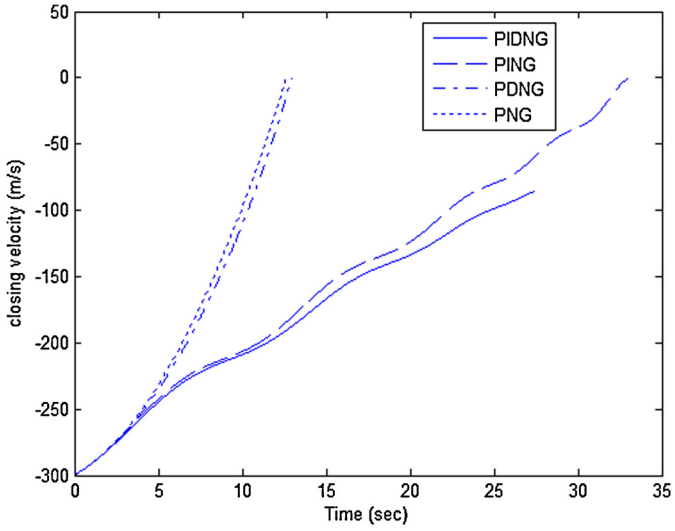

Fig. 11. The closing velocity.

$a_{T\theta} = 30$ m/s^2 and $a_{T\phi} = 30$ m/s^2. The stop condition is zero miss distance or failing to hit, i.e. $\dot{R} > 0$. The autopilot's parameters are $\zeta = 0.4$, $\tau_1 = 1$, and $\omega_n = 30$. Coefficients of new guidance are $K_1 = 3$, $K_2 = 1$, and $K_3 = 2$.

In this work, only results of azimuth loop have been shown because both elevation loop and azimuth loop are almost similar. Figs. 11–13 show the closing velocity, the LOS rate, and the acceleration command in azimuth loop, respectively.

According to Fig. 11 we see that sign of closing velocity for PNG, PING and PDNG changed and it became positive and the simulation stopped, but for PIDNG it remains negative, so only proposed guidance law can hit the target and other guidance laws failed.

The LOS angular rate has been shown in Fig. 12. As it can be seen, under the proposed law, the LOS angular rate remains at vicinity of zeros. Fig. 13 indicates the acceleration command. It is clear that although the proposed law is the only successful one to hit the target, but the maximum acceleration command of the proposed law is lower than that of even PING. This scenario confirms that the proposed law is better than PNG, PDNG and PING in terms of robustness and effectiveness.

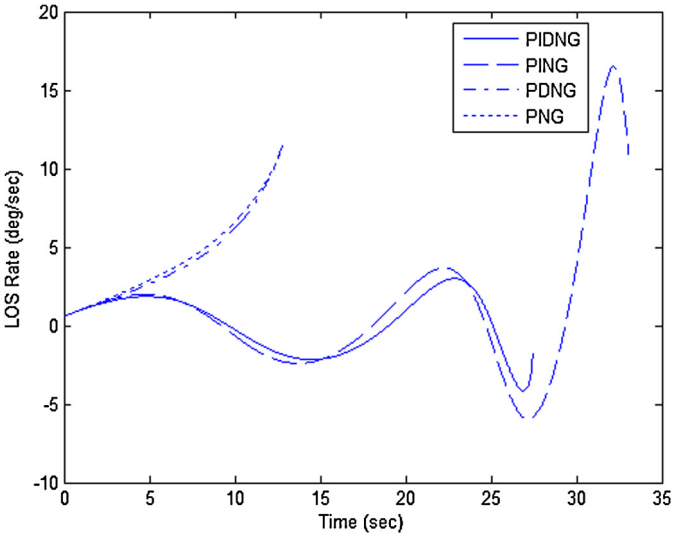

Fig. 12. The LOS rate in azimuth loop.

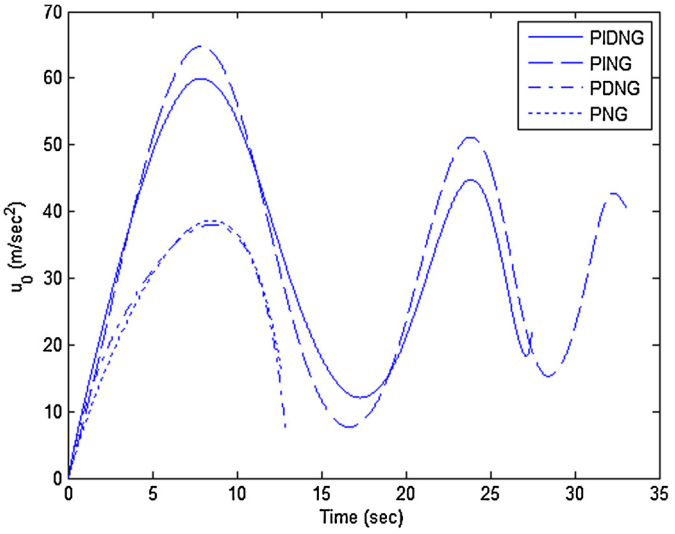

Fig. 13. The acceleration command in azimuth loop.

7. Conclusion

In this work, a new proportional-integral-derivative (PID) navigation guidance law was presented and the stability analysis considering dynamics of the seeker and autopilot was investigated utilizing the circle criterion. Since the guidance issue is a finite time problem, the lower bound of the guidance loop's stability was obtained based on the time to go, for finite flight time, using circle criterion. These conditions can be used to design coefficients of guidance law and suitable determination of parameters of seeker and autopilot. The lower bound of stability for the new guidance law is less conservative than PNG, PDNG and PING, and it has a larger stability range. Three-dimensional nonlinear simulation results show that the stability region is more than PNG, PDNG and PING.

Conflict of interest statement

None declared.

Appendix A. Proof of Lemma 1

To prove Lemma 1, the following lemma should be introduced.

Lemma 2. *Consider two polynomials $a(z)$ and $b(z)$ with $\deg a(z) < \deg b(z)$, and four constants c_1, c_2, c_3 and c_4 with $c_1c_4 - c_2c_3 \neq 0$, then the polynomials $c_1a(z) + c_2b(z)$ and $c_3a(z) + c_4b(z)$ are coprime [3].*

Using Eq. (14)

$$sq(s) = -2sd(s) + \left(K_3s^2 + K_1s + K_2\right)n(s) \tag{A.1}$$

$$p(s) = sd(s) \tag{A.2}$$

Since $n(s)$ and $d(s)$ are coprime, in order to have $sd(s)$ and $(K_3s^2 + K_1s + K_2)n(s)$ coprimed, they should not have common roots, so Eqs. (16) and (17) should be satisfied. If these two terms are coprime, based on Lemma 2, $p(s)$ and $sq(s)$ are coprime, too. Also if $K_2 \neq 0$, then $K_2n(0) \neq 0$, and by Eqs. (A.1) and (A.2), $p(s)$ and $q(s)$ are coprime.

Appendix B. Supplementary material

Supplementary material related to this article can be found online at http://dx.doi.org/10.1016/j.ast.2015.02.016.

References

[1] P.F. Curran, Proof of the circle criterion for state space system via quadratic Lyapunov functions — Part 2, Int. J. Control 57 (4) (1993) 957–969.
[2] P. Gurfil, Zero miss distance guidance law based on line of sight rate measurement only, Control Eng. Pract. 11 (7) (2003) 819–832.
[3] P. Gurfil, M. Jodorkovsky, M. Guelman, Finite time stability approach to proportional navigation system analysis, J. Guid. Control Dyn. 21 (6) (1998) 853–861.
[4] P. Gurfil, M. Jodorkovsky, M. Guelman, Neoclassical guidance for homing missiles, J. Guid. Control Dyn. 24 (3) (2011) 453–459.
[5] A. Koren, M. Idan, O.M. Golan, Integrated sliding mode guidance and control for a missile with on–off actuators, J. Guid. Control Dyn. 31 (1) (2008) 204–214.
[6] N. Lechevin, C.A. Rabbath, Lyapunov based nonlinear missile guidance, J. Guid. Control Dyn. 27 (6) (2005) 1096–1102.
[7] K.Y. Lum, J.X. Xu, K. Abidi, H. Xu, Sliding mode guidance law for delayed LOS rate measurement, in: AIAA Guidance, Navigation and Control Conference and Exhibit, Honolulu, Hawaii, 2008.
[8] I. Mohammadzaman, H. Momeni, PI guidance law design using circle criterion, J. Control 4 (2) (2010) 11–19.
[9] J. Moon, K. Kim, Y. Kim, Design of missile guidance law via variable structure control, J. Guid. Control Dyn. 24 (4) (2001) 659–664.
[10] S. Pardeep, S.K. Shrivastava, Stability of dynamic systems: an overview, J. Guid. Control Dyn. 13 (3) (1990) 385–393.
[11] D.Y. Rew, M.J. Tahk, H. Cho, Short time stability of proportional navigation guidance loop, IEEE Trans. Aerosp. Electron. Syst. 32 (4) (1996) 1107–1115.
[12] T. Shima, M. Idan, O.M. Golan, Sliding mode control for integrated missile autopilot guidance, J. Guid. Control Dyn. 29 (2) (2006) 250–260.
[13] N.A. Shneydor, Missile Guidance and Pursuit; Kinematics, Dynamics, Horwood Series in Engineering Science, 1998.
[14] Y.B. Shtesell, I.A. Shkolnokov, Integrated guidance and control of advanced interceptors using second order sliding modes, in: Proceedings of 42nd IEEE Conference on Decision and Control, Maui, Hawaii, USA, 2003, pp. 4587–4592.
[15] Y.B. Shtesell, C.H. Tournes, Integrated higher-order sliding mode guidance and control for dual-control missiles, J. Guid. Control Dyn. 32 (6) (2009) 1838–1846.
[16] C.D. Yang, C.C. Yang, Analytical solution of three-dimensional realistic true proportional navigation, J. Guid. Control Dyn. 19 (3) (1996) 569–577.
[17] R. Yanushevsky, Concerning Lyapunov based guidance, J. Guid. Control Dyn. 29 (2) (2006) 509–511.
[18] R. Yanushevsky, W. Boord, Lyapunov approach to guidance law design, Nonlinear Anal. 63 (5) (2005) 743–749.
[19] R. Yanushevsky, W. Boord, New Lyapunov approach to guidance law design, J. Guid. Control Dyn. 28 (1) (2005) 162–166.
[20] P. Zarchan, Tactical and Strategic Missile Guidance, AIAA Series, 2002.
[21] D. Zhou, S. Sun, K.L. Teo, Guidance laws with finite time convergence, J. Guid. Control Dyn. 32 (6) (2009) 1838–1846.